A combined field/remote sensing approach for characterizing landslide risk in coastal areas.

Mirko Francioni (a*)(b), John Coggan (b), Matthew Eyre (b), Doug Stead (c),
a) Department of Engineering and Geology, University of Chieti-Pescara, Chieti, Italy
b) Camborne School of Mines, University of Exeter, Penryn, Cornwall, UK
c) Department of Earth Sciences, Simon Fraser University, Burnaby, BC, Canada
Corresponding author: Mirko Francioni (m.francioni@exeter.ac.uk)
*Present affiliation

Abstract

Understanding the key factors controlling slope failure mechanisms in coastal areas is the first and most important step for analyzing, reconstructing and predicting the scale, location and extent of future instability in rocky coastlines. Different failure mechanisms may be possible depending on the influence of the engineering properties of the rock mass (including the fracture network), the persistence and type of discontinuity and the relative aspect or orientation of the coastline. Using a section of the North Coast of Cornwall, UK, as an example we present a multi-disciplinary approach for characterizing landslide risk associated with coastal instabilities in a blocky rock mass.

Remotely captured terrestrial and aerial LiDAR and photogrammetric data was interrogated using Geographic Information System (GIS) techniques to provide a framework for subsequent analysis, interpretation and validation. The remote sensing mapping data was used to define the rock mass discontinuity network of the area and to differentiate between major and minor geological structures controlling the evolution of the North Coast of Cornwall.

Kinematic instability maps generated from aerial LiDAR data using GIS techniques and results from structural and engineering geological surveys are presented. With this method, it was possible to highlight the types of kinematic failure mechanism that may generate coastal landslides and highlight areas that are more susceptible to instability or increased risk of future instability. Multi-temporal aerial LiDAR data and orthophotos were also studied using GIS techniques to locate recent landslide failures, validate the results obtained from the kinematic instability maps through site observations and provide improved understanding of the factors controlling the coastal geomorphology. The approach adopted is not only useful

for academic research, but also for local authorities and consultancy's when assessing the likely risks of coastal instability.

Key words: Remote sensing, Landslide risk, LiDAR, GIS, Coastal instabilities, Listric faults

1 Introduction

Discontinuity-controlled slope instabilities are an important natural hazard that can affect hard rock coastlines in blocky rock masses. Different failure mechanisms may be kinematically feasible depending on the influence of the rock mass fracture network (geometry and engineering characteristics of identified fracture sets that form a three dimensional fracture network) and the relative orientation of the coastline to the fracture network. The study of coastal failure involves evaluation of several contributing factors such as underlying failure and erosion mechanisms, changes in environmental (weather and sea) conditions, variations in coastline morphology, geology and structural geology, etc. (Collins and Sitar, 2008; Wolters and Müller, 2008; Abellán et al. 2009; Naylor et al., 2010; Stock et al., 2012). The analysis and prediction of such failures can be challenging as it is also important to consider the spatial and temporal aspects of failure as well as scale, size, impact and consequence.

Several recent studies have identified the potential use of remote sensing techniques for improved understanding of coastal processes, although most investigations are associated with relatively small scale studies. For example, at a scale of several kilometres Rosser et al. (2013) showed the use of multi-temporal terrestrial laser scanning for analyzing precise failure patterns across near-vertical rock cliffs on a section of the UK North Sea coast. Although the precise patterns highlighted by their research is specific for the site studied, the underlying progressive incremental failure mechanism proposed can be applied to wider applications. More recently, Mantovani et al. (2016) highlighted the use of InSAR techniques and developed a methodology for automatic classification of radar reflectors phase histories. Using this approach, the authors were able to interpret the kinematics and displacement trends of slow-moving coastal landslides in a sector of the island of Malta. The combined use of InSAR and UAV techniques is described by Mateos et al. (2017) for monitoring of a landslide affecting the urban development in the Cármenes del Mar Resort.

When applying these techniques to a larger/regional scale a wider area has to be studied and more information considered. Application of InSAR can be often be problematic because of the absence of natural scatter areas, presence of vegetation, unavailability of images, unsuitable satellite return periods, cost and complexity of post-processing. Dickson and Perry (2016) recently presented the use of a machine-learning approach for analyzing coastal cliff landsliding in a large portion of New Zealand using an existing landslide database containing 498 landslides. This purely-statistical based research (where cliff and bedding geometry, lithologies, slope degree/aspect/exposure and proximity to faults were used as predictors) highlighted that in the studied area, landsliding generally occurs at sites where faults intersect cliffs with high slope angle.

In this paper, we provide a regional scale analysis of coastal instability that includes identification of recent landslides and highlights the influence of structural geology on the likely scale of potential instability. This is performed using conventional predictors (such as cliff and bedding geometry, lithologies, slope degree/aspect/exposure) with information relating to the structural setting of the area (type and shape of faults and fracture sets). We use a section of the North Coast of Cornwall, UK (Figure 1A), between Hell's Mouth and Portreath, shown in Figure 1B, to demonstrate how the combined use of several disciplines (geology, structural geology, GIS, remote sensing) provided a multi-scale analysis of coastal instability in blocky rock masses. Specifically, the proposed multi-disciplinary approach emphasizes the integrated use of conventional geological/engineering surveys, aerial and terrestrial remote sensing and GIS together with validation through engineering geological mapping and site observations. Special emphasis is given to the evaluation of the role of major faults in controlling the volume/type of failures and the geometry or geomorphology of the coastline. Two 'site-specific' investigations showing the importance of structural geology in the analysis of slope failures are illustrated by Humair et al. (2013) and Brideau et al. (2009) in the analysis of the Turtle Mountain (Alberta, CA), Hope Slide (British Columbia, CA) and Randa Rockslide (Switzerland). Using a similar approach, this has been extended in the current research to a more regional scale study.

Figure 1. A) 3D Google Earth image of Cornwall with study area highlighted in black (inset shows a map of United Kingdom with Cornwall highlighted in red). B) Area of study between Hell's Mouth and Portreath on the North Coast of Cornwall.

Aerial LiDAR and photogrammetry were used to identify major structures in the study area. This data was then integrated with field data (traditional engineering geological and remote sensing surveys) to generate a discontinuity database that included both major and minor structures.

GIS was used in this study to improve the interpretation of remote sensing data and develop kinematic instability maps. Other research showing the use of GIS and remote sensing in landslide and structural geology investigations has been presented by Jaboyedoff et al. (2004), Oppikofer (2009), Brideau et al. (2011), Fey et al. (2015) and Francioni et al. (2015), (2017a).

Finally, to identify recent landslides that have occurred in the immediate area of study and validate the results obtained from the GIS analysis, two aerial LiDAR datasets, 2011 and 2014 (available through Channel Coastal Observatory, 2017), were compared and the results used to locate failures that occurred during this period. Analysis of the LiDAR datasets confirmed that the Hell's Mouth failure (September 2011) was the most significant landslide event in the area during this time and that the characteristics of the landslide are likely to be controlled by the structural geology of the area.

Although the specific results/patterns obtained/identified should be considered specific for the area under investigation, the use of the proposed methodology, combined with techniques suggested by previous research (Collins and Sitar, 2008, 2011; Naylor et al., 2010; Rosser et al. 2013), provides new insight into the study of rocky coastline evolution. The research identifies the challenge of large scale spatial analysis in determining areas of potential failure, and the role of structural geology on coastal instability. The approach adopted is not only useful for academic research, but also for local authorities and consultancy's when assessing the likely risks of coastal instability.

2 Study area

2.1 Landslide Characteristics

This research study is focused on a section of the North Coast of Cornwall, UK, between Hell’s Mouth and Portreath. This section of coastline is known to be susceptible to landslide activity: varying from low volume rock fall to entire cliff collapse (Jones et al., 1998; Shail et al., 1998; British Geological Survey, 2017; Westgate, 2005; Westgate et al., 2003).

One of the more recent instabilities occurred on the afternoon of Friday 23rd September 2011 immediately adjacent to Hell’s Mouth. The landslide was captured on video and is recorded in the British Geological Survey Landslide Database (British Geological Survey, 2017). Although this landslide is commonly referred to as the ‘Hell’s Mouth’ failure, it is actually located at Hudder Cove, immediately to the East of Hell’s Mouth. A jogger reported a large crack in the coastal path 5 days prior to failure. This prompted Cornwall Council (working alongside the landowners The National Trust) to divert the coastal path for public safety. Following the early identification, surveys by Cornwall Council were undertaken observing further tension crack development, one day prior to failure. On Friday 23 September 2011, reports of material falling from the cliff were noted throughout the day with the slope failure captured on video at 4.50 p.m. (British Geological Survey, 2017).

Figure 2 shows that the Hell’s Mouth instability was associated with two major episodes of instability. The initial failure captured on video was subsequently followed by later failure of the section of the coastline immediately to the south of the original failure (cliff face dipping towards the west).

Figure 2. Photographs of Hell's Mouth failure area prior to failure and two subsequent episodes of instability. Comparison of photographs taken on 23/09/2011 and 24/12/2011 show further instability of the South-West section of the failure area a few weeks after the main landslide that was captured on video (photograph taken looking towards SSE).

2.2 Geological Setting

The South West of England is characterized by a series of interconnecting sedimentary basins, which developed sequentially northwards in the region during Early-Devonian to Mid-Devonian continental rifting (Leveridge and Hartley, 2006). The study area coincides with the location of the Gramscatho Basin which represents the earliest of these basins that was developed as a result of syn-rift sedimentation within graben and half-graben structures (Leveridge, 2011). The geology of the study area is dominated by the Porthtowan Formation, a 2.8 km thick Devonian metasedimentary sequence (Leveridge and Shail, 2011) composed of alternating beds of strong to moderately strong, medium to thinly bedded dark grey mudstone, interbedded with strong to moderately strong, thick to thinly bedded pale grey fine sandstone which may locally have a silt and mud component (Hollick et al., 2006). Discontinuities within this formation are characterized by low to medium/high persistence and smooth planar surfaces with local calcite and quartz infill. Joints may also enclose up to 3 mm thickness of dark grey clay infill originating from weathered slope profiles (Westgate, 2005).

Regarding the tectonic evolution of the area, in relation to what is observed in the field and in accordance with Alexander and Shail (1995) and Hughes et.al. (2009), two generations of North-North-West verging Variscan structures (Hercynian, related to late Paleozoic continental collision between Euramerica and Gondwana associated with Deformation phase 1 and 2 - D1 and D2) are post-dated by structures showing South-East sense of shear (deformation phase 3 - D3). Dl is evident at most localities and is marked by folds which verge North-North-West and a pervasive and penetrative cleavage, sub-parallel to bedding (S0) dipping gently South-South-East. D2 folds are close to tight asymmetric structures which verge North-North-West and are generally coaxial with D1 structures (Alexander and Shail, 1995). The axial planar cleavage to these folds dips at moderate to steep angles to the South-South-East. D3 represents an important phase with a switch in the dominant fold vergence towards the South or South-East. During this phase, there is a transition from a ductile to a more brittle regime related to the development of listric and predominantly low angle South-South-East dipping (10°-70°) extensional faults. Listric faults represent one of the most common indicators of an extensional regime. The main difference between these faults and frequently observed normal faults is their concave surface and for this reason they could be also defined as curved normal faults.

The NNW-SSE late orogenic extension started during D3 and continues after this phase with the generation of low angle North-North-West dipping listric faults and subsequently with steeper structures dipping either to the North-North-West or South-South-East.

This dominant North-North-West South-South-East extension probably lasted well into the Permian, and subsequently changed to approximately an East-West extension during the Triassic. In this regime, steep faults striking North-North-East or South-South-West were formed.

3 Methods

3.1 Engineering geological and terrestrial remote sensing survey

Engineering geological surveys have been carried out in two accessible and representative sections of the coastline within the study area. Two hundred discontinuities (joints, veins and faults) and their characteristics (trace length, spacing and surface description) were collected during the survey.

The cliffs on the section of coastline between Hell's Mouth and Portreath are up to 80 m high and have complex morphology. In such an environment, conventional engineering geological surveys can be extremely hazardous and difficult to perform and may only be possible for limited areas during low tides. In view of limited safe access, a photogrammetric survey of the Hell's Mouth failure region was undertaken to verify the structural setting, confirm the data from the engineering geology survey and increase the number of discontinuities to be used for defining the discontinuity sets present within the study area.

The photogrammetric survey was carried out from the headland to the West of Hell's Mouth (Hell's Mouth failure area highlighted in Figure 1) using a tripod and a Canon 50D with an $f = 200$ and $f = 400$ mm lens. The software Photoscan (Agisoft, 2016) was used to create the 3D model using Structure from Motion (SfM). Figure 3 shows a photograph of the 'Hell's Mouth' cliff before (Figure 3A) and after (Figure 3B) the failure, and the subsequent 3D photogrammetric model of the cliff after failure (Figure 3C).

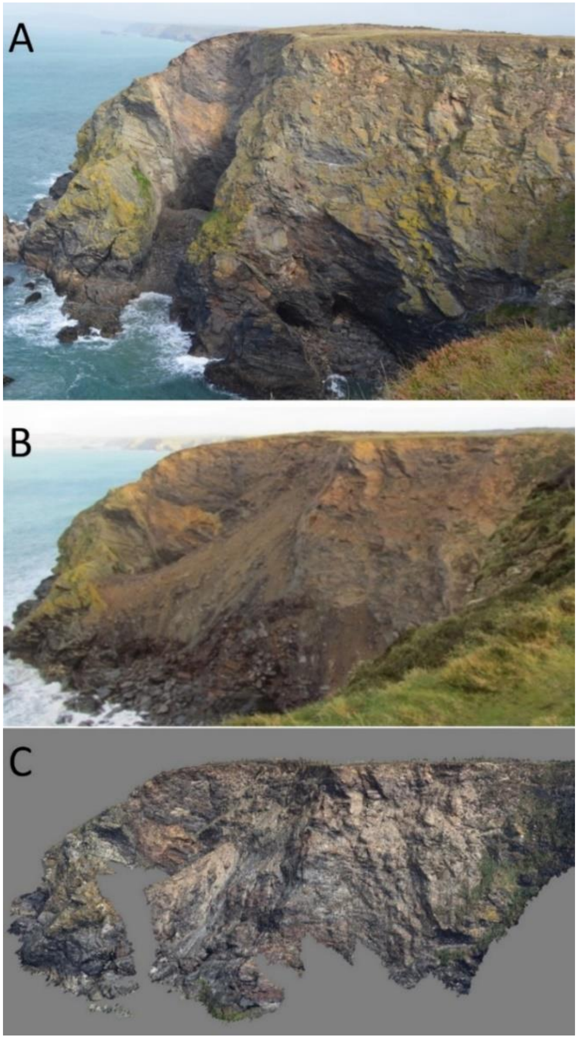

Figure 3. Images of Hell's Mouth landslide location. A) Photograph of Hell's Mouth cliff section taken before the 2011 failure. B) Photograph of Hell's Mouth after the 2011 failure. C) 3D SfM photogrammetric model of the cliff after failure (photograph taken looking towards SSE).

The software Split FX (Split Engineering LLC., 2016) was used for subsequent interrogation of the three-dimensional point cloud. Using this software, it was possible to extract geological structure from the point clouds (including discontinuity orientation and spacing) and plot the data on a stereonet for comparison with the conventional engineering geology data.

3.2 Aerial remote sensing and GIS analysis

Aerial LiDAR surveys are capable of rapidly collecting large volumes of point cloud data to a height accuracy of approximately 50 mm.

One of the main advantages offered by this technique is the ability to penetrate the vegetation cover, avoiding occlusions in the resulting dataset. Although LiDAR allows data acquisition over large areas, it may not always be suitable for the study of natural and artificial rocky slopes characterized by very steep or even vertical slope sections (Francioni et al., 2017b). In such cases, other techniques of analysis are suggested such as terrestrial laser scanning and digital terrestrial photogrammetry (DTP) (Rosser et al., 2005; Rosser et al., 2013; Francioni et al., 2017b). In this research, LiDAR has been combined with DTP for study of steep coastal slopes/cliffs. This data has a resolution of 1 m and covers the North Coast of Cornwall (including the current area of interest).

GIS was used to manage aerial LiDAR data and create thematic maps to facilitate identification and interpretation of structural and geomorphic features. Data obtained from engineering geology field work and LiDAR data was integrated with complementary data obtained from terrestrial remote surveys carried out in inaccessible areas directly related to this research.

3.2.1 <u>Major structural features and coastline analysis</u>

Persistent fault systems play a key role in the stability of the coastlines and can be defined as 1st order structures while joint sets, with lower persistence, can be defined as 2nd or lower order structures depending on their influence on stability.

Using the GIS software ESRI’s ArcMap version 10.2 (ESRI, 2016) it was possible to process the LiDAR data and generate thematic maps, such as a ‘hillshade’ map. A hillshade map is generated using a lighting effect based on differences in elevation within the landscape. It provides synthetic three-dimensional views of the landscape. This map was used in this study to identify by visual inspection/interpretation the major structures in the area. With the goal of verifying the possible relationship between structural features and coastline geometry the coastline was digitized in ESRI’s ArcMap (Figure 9C), and the respective azimuths calculated. Since the software calculates the azimuth of each segment, irrespective of their length, coastline segments were "normalized". The segments were given a set length of 100 m, avoiding preferential weighting (i.e. a segment length of 1 km does not have the same weighting as that of a 100 m segment).

3.2.2 GIS kinematic analysis

Kinematic analysis examines the likelihood that rock slope failures such as planar, wedge, and toppling will occur due to the presence of unfavorably oriented discontinuities. Although a very simple analysis it is a useful functional preliminary tool providing a first estimation of potential for failure (Jaboyedoff et al., 2004; Francioni et al., 2015).

The kinematic instability test considers the orientation of the discontinuities, the slope orientation and effective friction angle along the discontinuity surface(s). In the case of coastal areas, where the orientation of slopes can vary considerably, the kinematic analysis should be performed for every change of slope direction. Since this procedure can be complex and time consuming using conventional techniques, data from the GIS analysis and engineering geological survey were integrated/combined to automatically create kinematic instability maps.

We adopted an approach similar to that proposed by Jaboyedoff et al. (2004), Oppikofer (2009), Brideau et al. (2011) and Francioni et al. (2015). The GIS thematic slope and the aspect maps were created using ESRI's ArcMap and show respectively the steepness or inclination and the dip direction of the slopes/structures. Information gained from these two thematic maps was then combined using GIS spatial analysis techniques into a database containing both slope inclination and aspect information. Using kinematic analysis rules that control rock slope failure (Markland, 1972; Hoek and Bray, 1981), the possible combinations of slope geometry (dip and dip direction) prone to kinematic failure were calculated (in this preliminary analysis a friction angle and a lateral limit of 30° were assumed).

3.2.3 Multi-temporal aerial LiDAR analysis

The two aerial LiDAR data sets (2011 and 2014), were compared using the software CloudCompare (CloudCompare v2.6, GPL software, 2016). CloudCompare is freeware software developed in 2006 for comparing 3D point cloud datasets. The software has the capability to report deviation between two-point cloud objects (elevation change) or assess the accuracy of computer generated surface meshes from the original dataset. In this research, the LiDAR images were converted into point clouds using ESRI ArcMap and then imported into CloudCompare for interpretation. The 2011 LiDAR data was used as the reference data for comparison between the two periodic point clouds (to observe any changes).

4 Results

4.1 Results from engineering geological and photogrammetric surveys

Structural, engineering geological and remote sensing surveys identified 5 main discontinuity sets. Figure 4 shows a lower hemisphere stereonet representing the poles of 200 discontinuities (joints, veins and faults) collected during the engineering geological survey. Low angle discontinuities dipping towards SE represent the identified bedding (S0).

Figure 5A shows a lower hemisphere stereonet representation of the 302 discontinuities measured from the photogrammetric analysis. From this data, it is possible to observe that the discontinuity pole distribution is similar to that obtained from the conventional engineering geological surveys. The datasets were then combined to identify the main discontinuity sets present within the study area (Figure 5B) and their associated characteristics (Table 1).

These 5 discontinuity sets mainly follow two trends (NW-SE and NE-SW) and can be directly related to the structural evolution of the area. In Section 2 it was noted that the transition from a ductile (D1 and D2 Phases) to a more brittle regime started during D3.

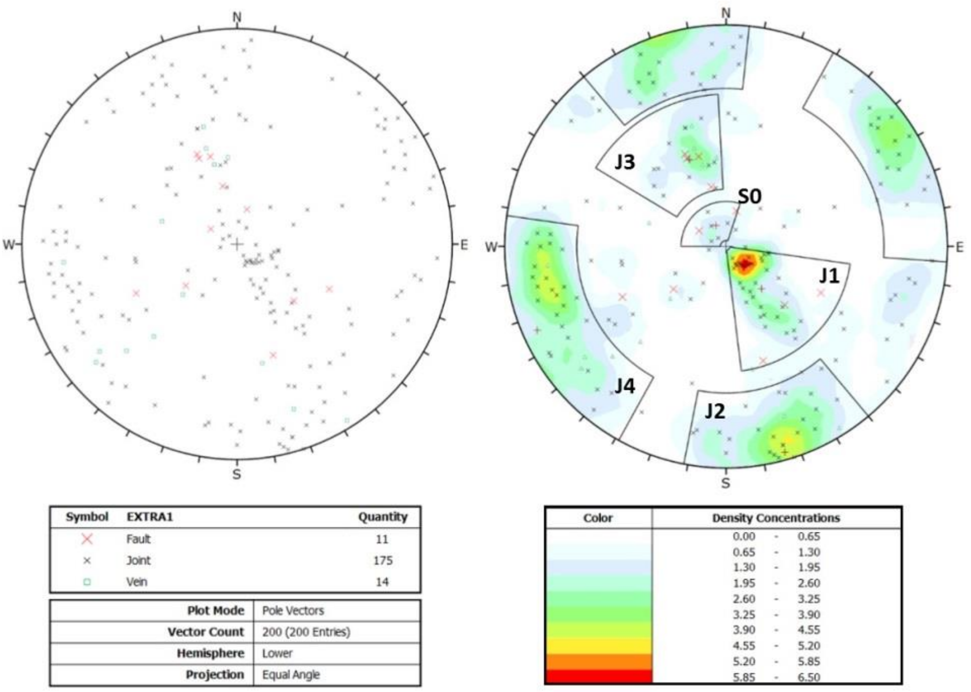

Figure 4. Stereonet representing 200 discontinuities collected during an engineering geological survey of a representative section of coastline within the study area.

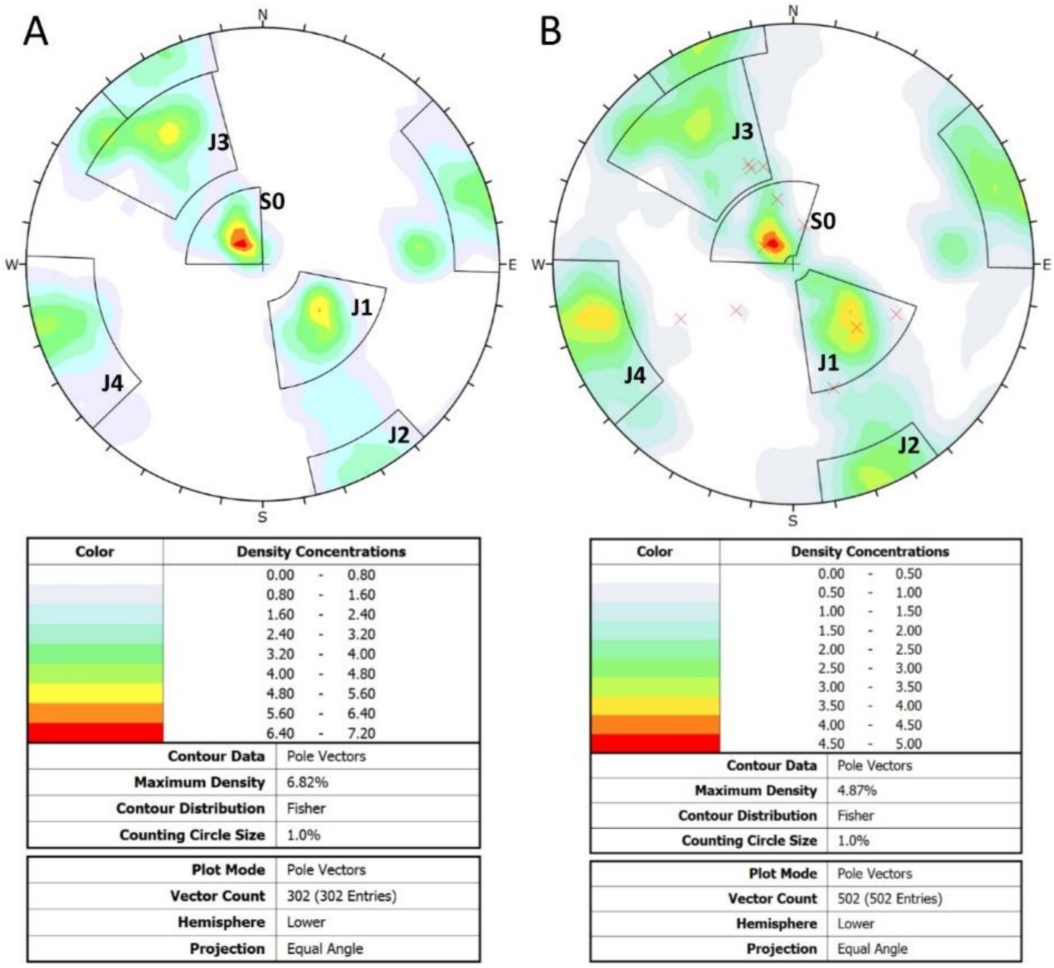

Figure 5. Lower hemisphere stereonets obtained from: A) the photogrammetric data, number of measurement equals 302; B) Combination of engineering geological mapping and photogrammetric data (number of measurement equals 502, red crosses highlight faults mapped during engineering geological survey).

Joint set	Eng. Geol. (Dip°/Dip Dir°)	DTP (Dip°/Dip Dir°)	Combined (Dip°/Dip Dir°)	Spacing (m)	Mean Trace length (m)	Description
S0	12/154	19/140	18/142	0.2 – 0.8	5.7	Bedding. Smooth, undulating, planar.
J1	28/320	37/317	34/320	0.3 – 1.5	2.8	Rough, undulating, stepped.
J2	88/344	90/332	87/336	0.3 – 1.5	3.2	Smooth, undulating, planar.
J3	46/157	65/142	64/143	0.3 – 1	4.2	Rough, undulating, planar.
J4	86/66	88/69	87/69	0.5 – 5	2.2	Smooth, undulating, planar.

Table 1. Characteristics of identified discontinuity sets and faults. Spacing and mean trace length refers to the joint sets only of the discontinuity sets identified in the stereonets using engineering geological data, DTP data and the combined data set.

During the first stage of D3 the formation of listric and predominantly low angle South-South-East dipping (10°-70°) extensional faults can be associated with the F3 system (Figure 6A). After D3, the extensional regime continued with the generation of low angle North-North-West dipping listric faults (F1 structures, Figure 6B) and subsequently with steeper structures dipping either to the North-North-West or South-South-East (F2 structures, Figure 6C). This extensional phase continued well into the Permian and then changed to approximately East-West extension during the Triassic forming high angle ENE or WSW dipping faults (F4 structures, Figure 6D). Table 2 provides the orientation of the four fault systems identified within the study area.

The mapping suggests that the joint sets are associated with four major fault systems (F1, F2, F3 and F4). F1 and F3 are characterized by listric faults, while F2 and F4 represent high angle normal faults. It should be noted that during the engineering geological survey it was not possible to acquire measurements of F2 and F4. This is because the engineering geological surveys have been undertaken in areas that were more easily and safely accessible. These fault systems are characterized by high dip angle and often do not daylight in the outcrops (i.e. fault dips at a higher angle than the cliff slope face angle). However, major lineaments attributable to F2 and F4 are observed in the photogrammetric and GIS analysis.

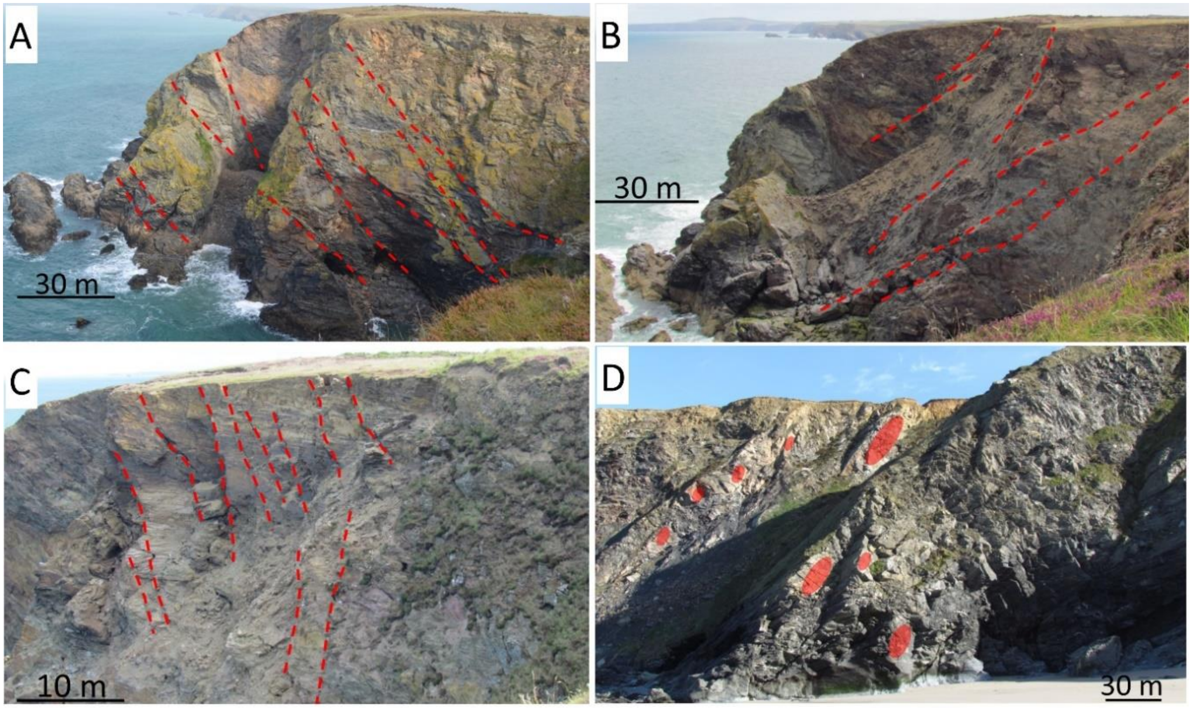

Figure 6. A) Photograph of Hell's Mouth failure area prior to failure with listric faults F3 (photograph taken looking towards NE). B) Photograph of Hell's Mouth failure area post failure with F1 (photograph taken looking towards NE). C) Photograph of Hell's Mouth failure area prior to failure with steep joint and fault structures J2 and F2 (photograph taken looking towards NE). D) Photograph of the section of coastline between Hell's Mouth and Basset's Cove showing F4 (photograph taken looking towards SSE).

Fault system	Strike	Dip°
F1 (listric)	NE	10°-60° (NW)
F2	ENE	Sub-vertical
F3 (listric)	NE	10°-70° (SE)
F4	NNW	Sub-vertical

Table 2. Orientation of the fault systems recognized in the study area

4.2 Representation of listric faults on a lower hemisphere stereonet

As previously described, F1 and F3 represent listric fault systems with dips varying from low (10°) to high (60° - 70°) angle. These fault systems play a key role in the evolution and stability of North Coast and for this reason, their study and representation are very important. However, the representation of listric faults on stereonet can be complicated and sometimes misleading due to the difficulty of visualization of the associated range of dip variation. One single measurement related to the dip of a listric fault would not be representative of the entire fault but only one specific point (dip will vary in relation to where the data is collected along the structure). In this context, a suggested methodology is provided to represent listric faults on a stereonet using, when available, the entire range of the measured fault's dip. Figure 7A shows the slope adjacent to the Hell's Mouth failure with a listric fault highlighted belonging to F1. Split-FX was used to take measurements from the orthorectified 3D model along the fault surface (Figure 7B). This data was then transferred onto the lower hemisphere stereonet (Figure 7C) and a best fit line/arrow drawn starting from the highest to lowest dip values (Figure 7D). The arrow provides information about the fault dip direction (direction of the arrow), the range of dip (from the beginning to the end of the arrow) and dip direction variation related to the waviness of the fault surface. When plotted on a kinematic stereographic analysis using a daylight envelope construction, it may then be possible to recognize potential bi-planar/multi-planar fault controlled mechanisms.

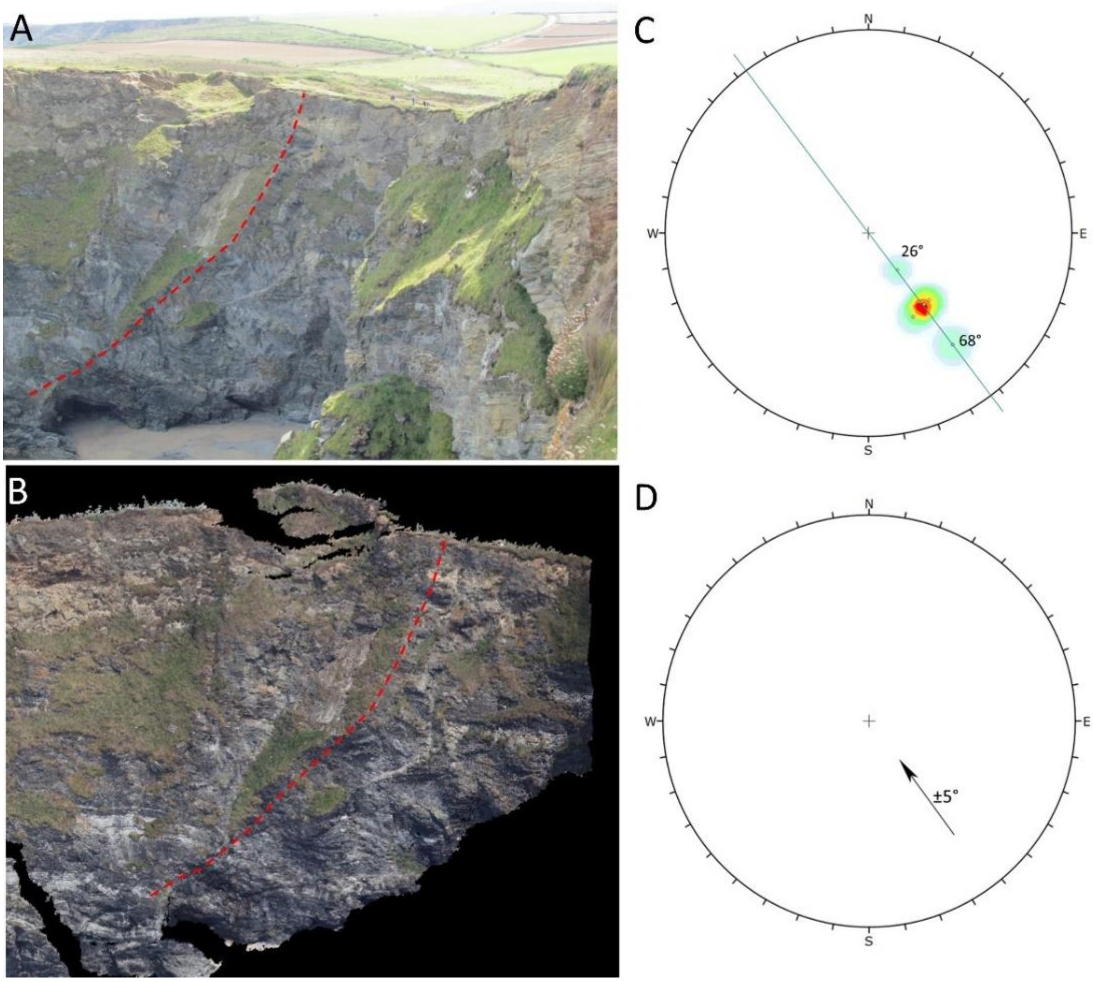

Figure 7. A) Listric fault highlighted in photograph. B) Photogrammetric 3D model of the area. C) Stereonet of five measurements of the listric fault surface measured in the 3D model, 26° and 68° are the lowest and highest dips measured along the fault. D) Proposed representation of a listric fault on the stereonet; 5° represents the dip direction variability measured in the 3D model.

4.3 Results from GIS analysis

The creation and interpretation of the 'hillshade' map (Figure 8A) within ArcGIS software was important to define the major lineaments in the study area (Figure 8B). The light angle used in Figure 8 has an azimuth of 315° (light cast from the northwest) and an inclination of 25°. However, different light angle/azimuth combinations have been used to avoid interpretation errors related to map lighting. The identified major structures were aligned along two main trend directions respectively: North-West (F4) and North East (F1 and F3), which coincides with the previously mapped discontinuity data that appear to control the geometrical evolution of the entire North Coast of Cornwall.

The GIS analysis of the coastline orientation, shown in Figure 8C, confirmed this alignment trend, highlighting how the coastline closely reflects the two main trends also observed in the discontinuity mapping.

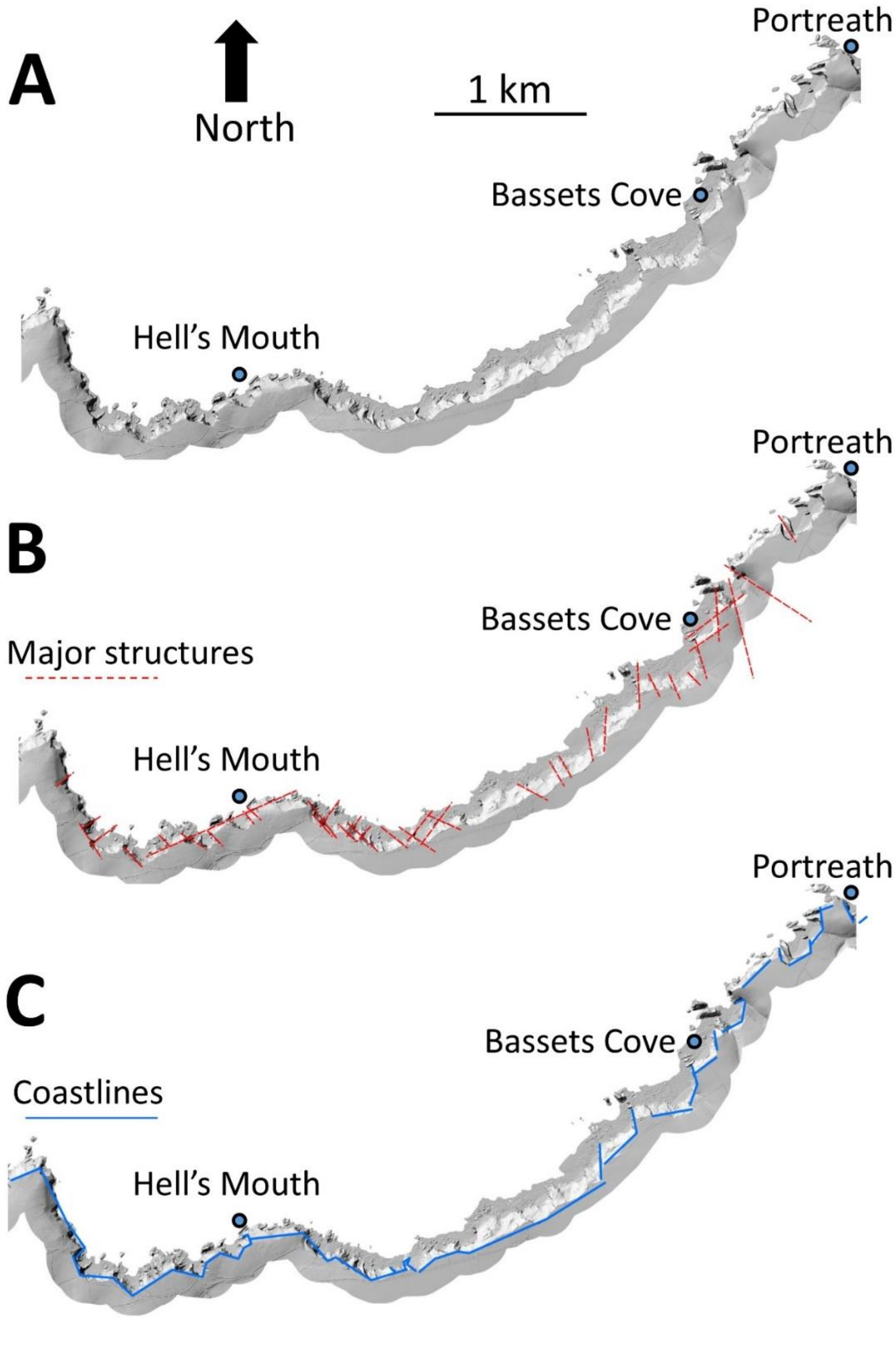

Figure 8. Hillshade analysis. A) Hillshade map. B) Major structures identified from interpretation of the hillshade map. C) Coastline orientation digitized on the hillshade map.

4.4 Results from multi-temporal analysis

The comparative analysis of 2011 and 2014 LiDAR data highlighted changes in coastline geometry during this period, including the major Hell's Mouth landslide that occurred in September 2011 and the relatively minor Basset's Cove failure. Figure 9 and Figure 10 show the results of the analysis related to the Hell's Mouth and Basset's Cove failures; with positive values indicating decreased elevation from 2011 and 2014 (possible instability or coastal recession) and negative values indicating increased elevation (possible material accumulation or deposition). Changes below 1 m were excluded at this stage of the analysis.

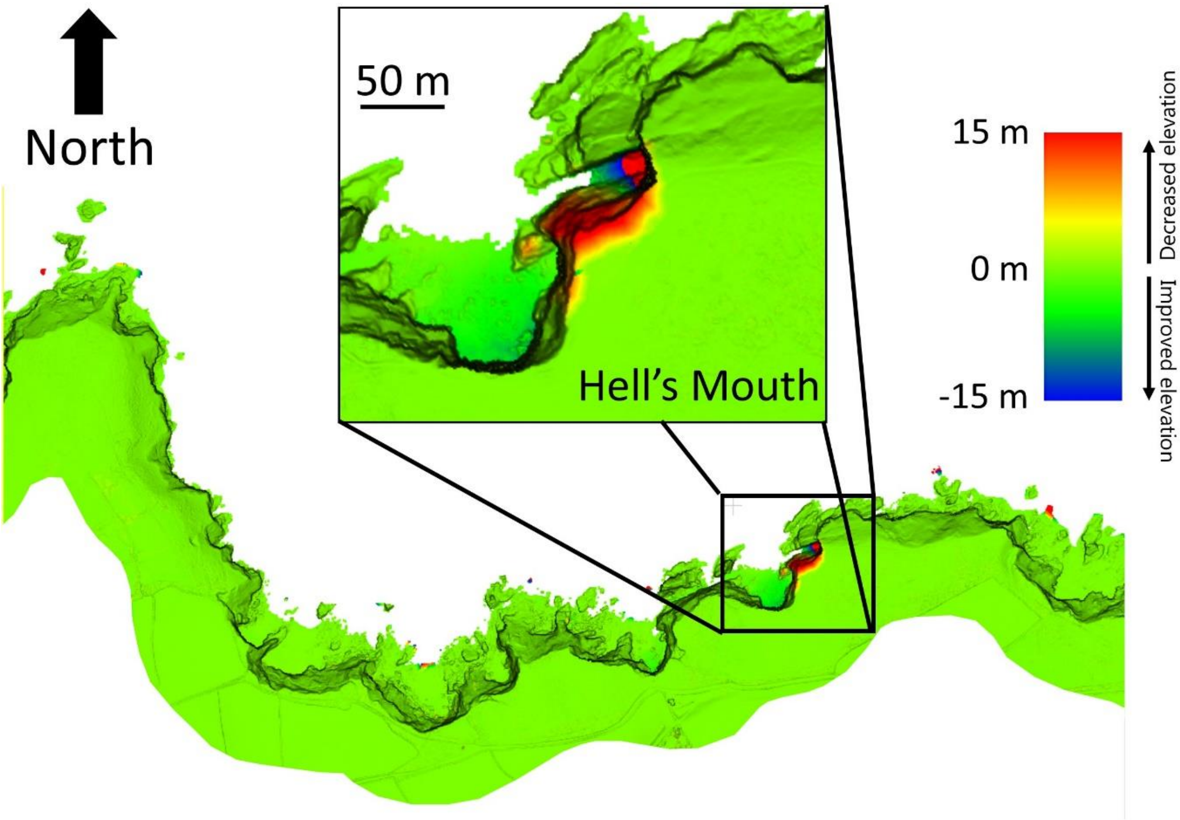

Figure 9. Results from comparison of 2011 and 2014 LiDAR data. Positive values indicate decreased elevation from 2011 and 2014 (possible instability or coastal recession) and negative values indicate increased elevation (possible material accumulation or deposition). The Hell's Mouth landslide area is highlighted in the inset.

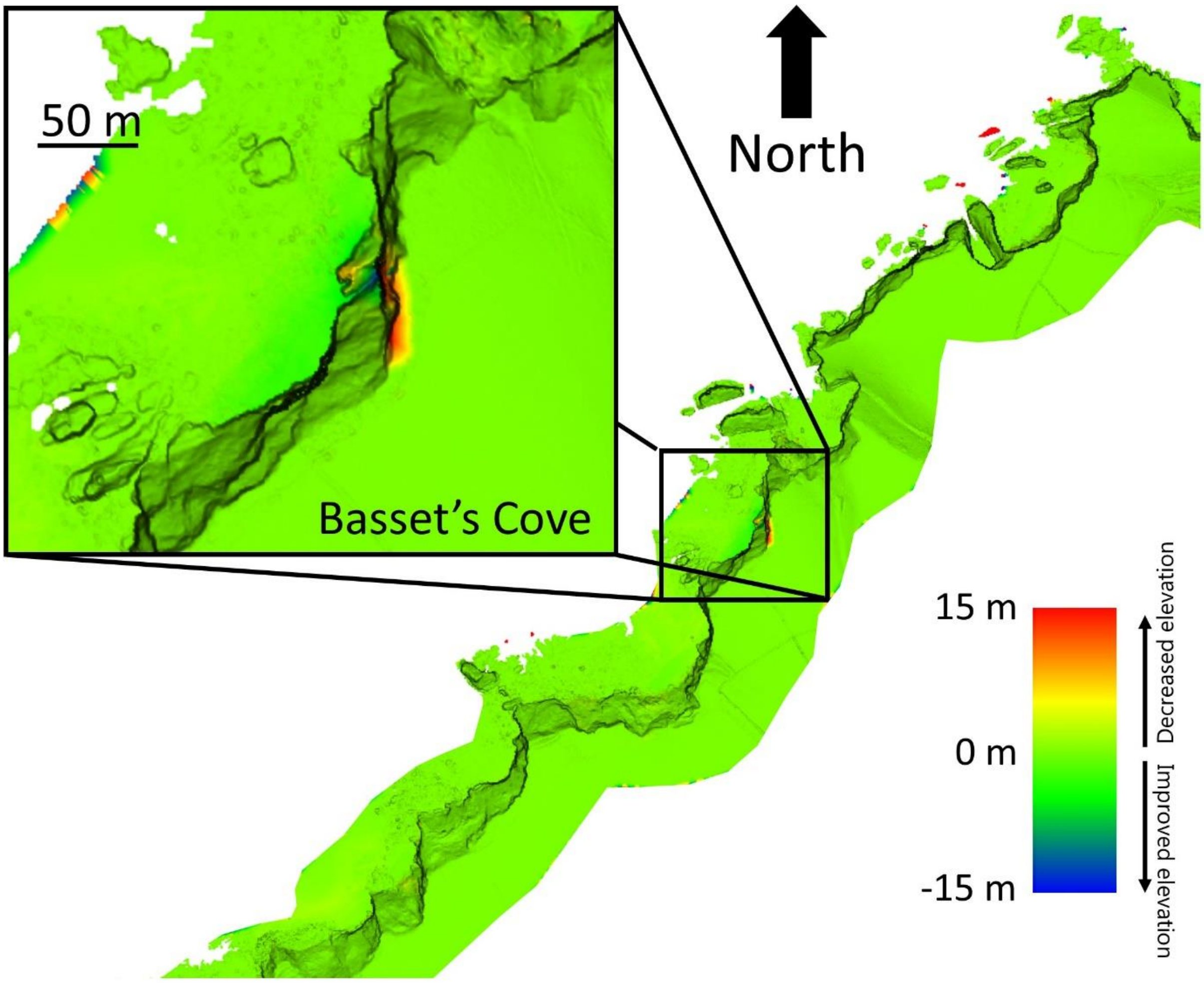

Figure 10. Results from comparison of 2011 and 2014 LiDAR data. Positive values indicate decreased elevation from 2011 and 2014 (possible instability or coastal recession) and negative values indicate increased elevation (possible material accumulation or deposition). The Basset's Cove failure is highlighted in the inset.

The Hell's Mouth landslide LiDAR data shown in Figure 9 can be compared with images, presented in Figures 2 and 11, of the immediate area before and after failure. These images show the development of a 'zawn' along a major fault F3 forming the northern boundary of the landslide area. A 'zawn' can be described as a deep and narrow sea-inlet in the British Isles, especially Cornwall and the south-west, cut by erosion into sea-cliffs with steep or near vertical side-walls. The aerial images presented in Figure 11 also show the slope before (Figure 11A) and after (Figure 11B) the failure highlighting the loss of the coastal footpath and it's re-routing away from the landslide. Tension crack development behind the failure scar can be clearly observed in the post failure image (Figure 11B and C). These cracks have extended post failure and are a clear indication of likely further instability.

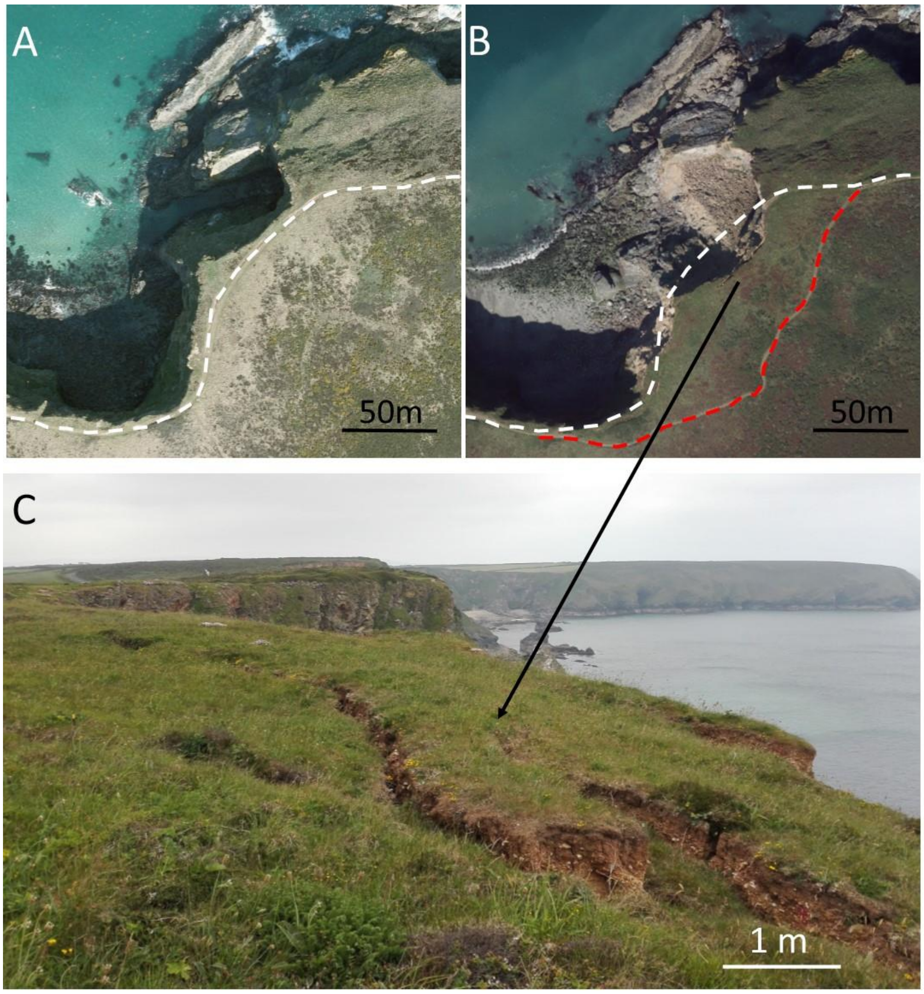

Figure 11. Ortho-rectified aerial photographs of Hell's Mouth landslide. A) Aerial Photograph before (2010) and (B) after failure (2013) - photographs from Channel Coastal Observatory (2017). C) Tension crack development behind the 2013 failure scar. White dashed line shows the location of the coastal footpath before the failure and the red dashed line showing re-routing following the landslide.

The tension cracks behind the failure scar were mapped both in the field and using the available ortho-photos and their azimuth plotted on a rosette diagram. These features are associated with the same trends as identified in the GIS analysis. Figure 12 shows the measurements related to the major lineament, coastline and tension crack orientations plotted on a rosette diagram (Figure 12A-C).

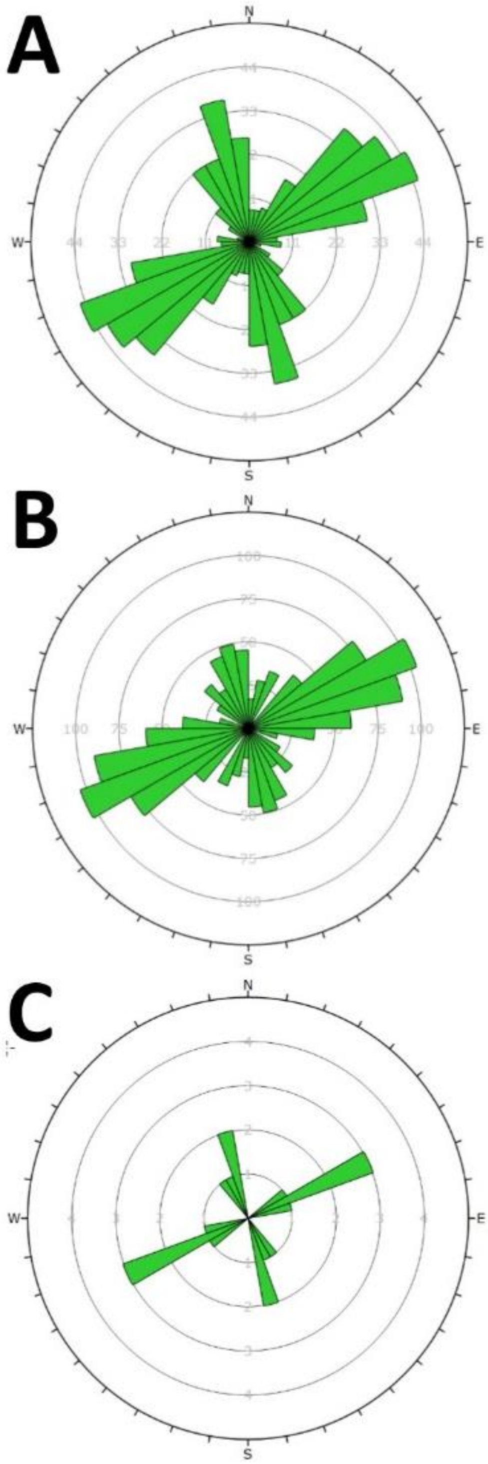

Figure 12. Rosette plots of major trends observed in structural/lineament data from the study area. A) Trends observed in discontinuity orientation data from engineering geology and remote sensing surveys. B) Coastline aspect analysis. C) Tension crack orientation analysis.

A study of photographs taken before and after the Hell's Mouth failure also show that this failure (Figure 2 and 6B) was influenced by F1 (listric faults with dip varying from 10° to

60°). F2 faults acted as potential tension cracks as observed immediately prior to the failure and have subsequently developed and extended post failure. F4 faults appear to act as lateral release surfaces. This suggests that evolution of the North Coast near Hell's Mouth is dominated by the structural geology of the area. Figure 13 shows the kinematic analysis of the Hell's Mouth failure highlighting the interaction between joints and faults and the potential role of the listric fault (mapped using DTP, Figure 6B) as a likely failure surface and F2/J2 and F4/J4 (interpreted by LiDAR analysis, Figure 8) as lateral release and tension crack surfaces.

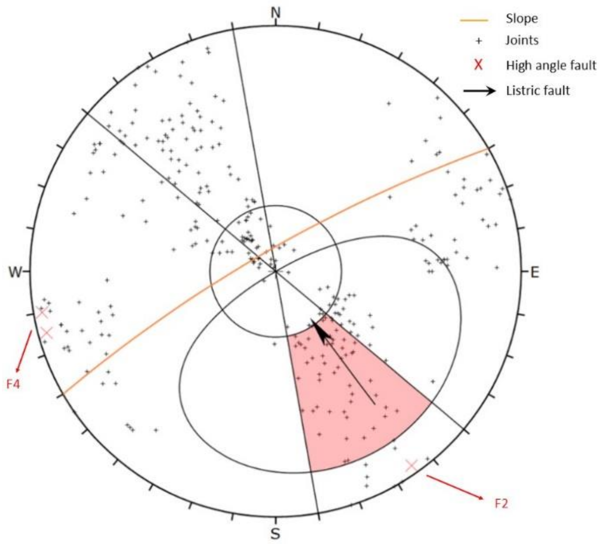

Figure 13. Kinematic analysis of the Hell's Mouth failure

Given the current tension crack growth, both in width and length, behind the failure scar there is an increased likelihood of further instability. Figure 14 provides a reconstruction of the Hell's Mouth failure: Figures 14A and 14B show the Hell's Mouth slope before and after the failure; Figure 14C shows the comparison of 2011 and 2014 LiDAR data of the Hell's Mouth failure highlighting the role of the structural geology and, finally, Figure 14D provides a conceptual 3D model of the failure using the Rocscience SWedge software (Rocscience, 2016). It should be noted SWedge does not allow modelling of listric (a surface with varying dip) faults and for this reason, F1 is shown in this simplified representation as a planar surface combining with F2 to form a biplanar wedge.

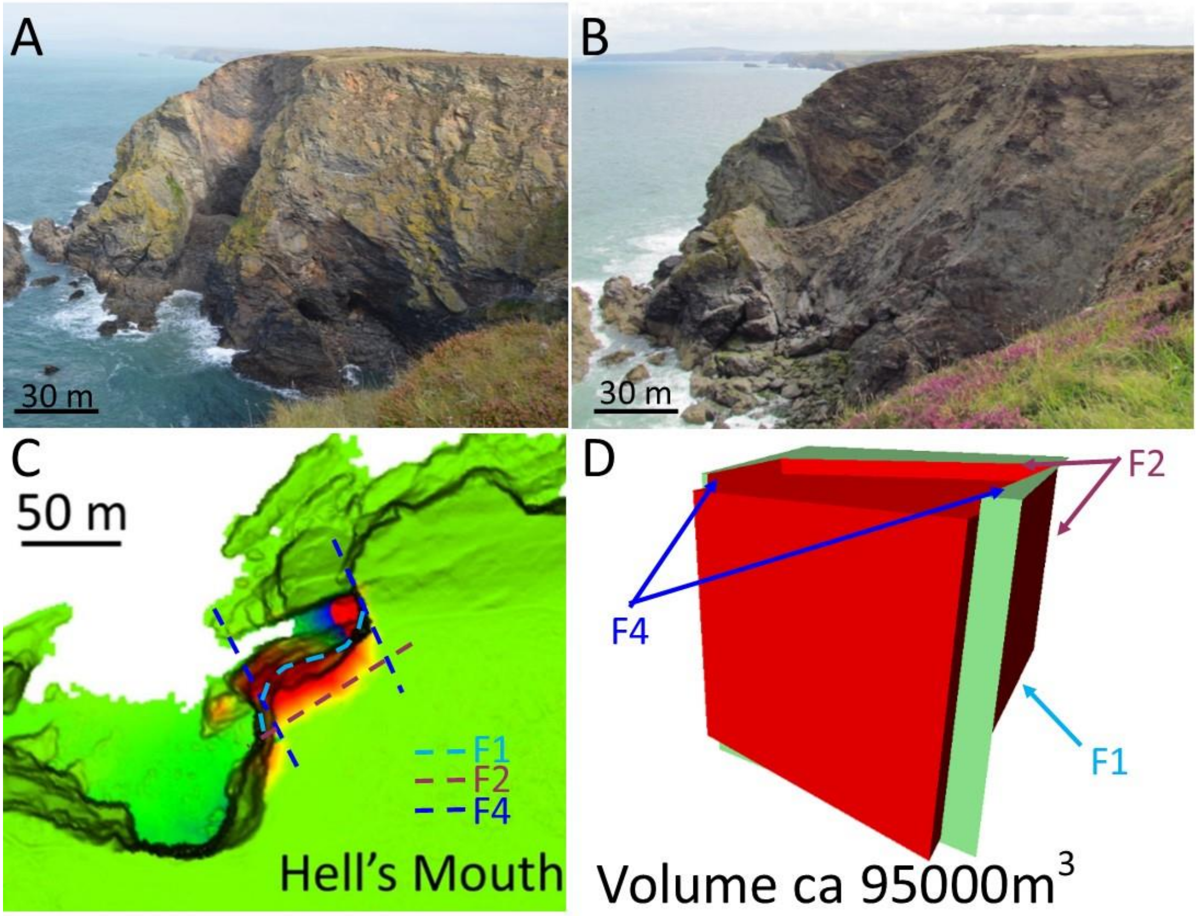

Figure 14. Hell's Mouth failure. A) Hell's Mouth slope before the failure (Photograph taken looking towards North-East). B) Hell's Mouth slope after the failure (Photograph taken looking towards North-East). C) Comparison of 2011 and 2014 LiDAR data and structural features. D) Conceptual 3D model of the failure (View looking towards South-East).

Regarding the minor failure detected by the LiDAR comparison at Basset's Cove (Figure 10), it can be seen in Figure 15 that this wedge failure occurred along F2/J2 and F4/J4. Figures 15A and B show the ortho-photographs before and after the failure. Figure 15C shows the 2011 and 2014 LiDAR comparison and, finally, Figure 15D shows a conceptual 3D failure model. The volume of this failure, ca 15000 m^3 (calculated with SWedge software), is much smaller than the failure that occurred at Hell's Mouth (ca. 95000 m^3). In this case listric faults (F1 and F3) do not daylight in the slope (dipping toward W) and the failures are associated with high angle failure surfaces F2 and F4 (without the interaction with lower angle dipping sets) that generate smaller failure volumes. This conceptual model is a simplified representation of the failure that may also have involved a series of smaller wedges/blocks or retrogressive failures associated with intersections between J2/F2 and J4/F4. For comparison purposes, 2.5D volume computations of the respective failures were undertaken in CloudCompare from the 2011 and 2014 LiDAR data. The calculated volume of the failure at Hell's Mouth was found to be approximately 75126 m^3 and Bassett's Cove 9850m^3.

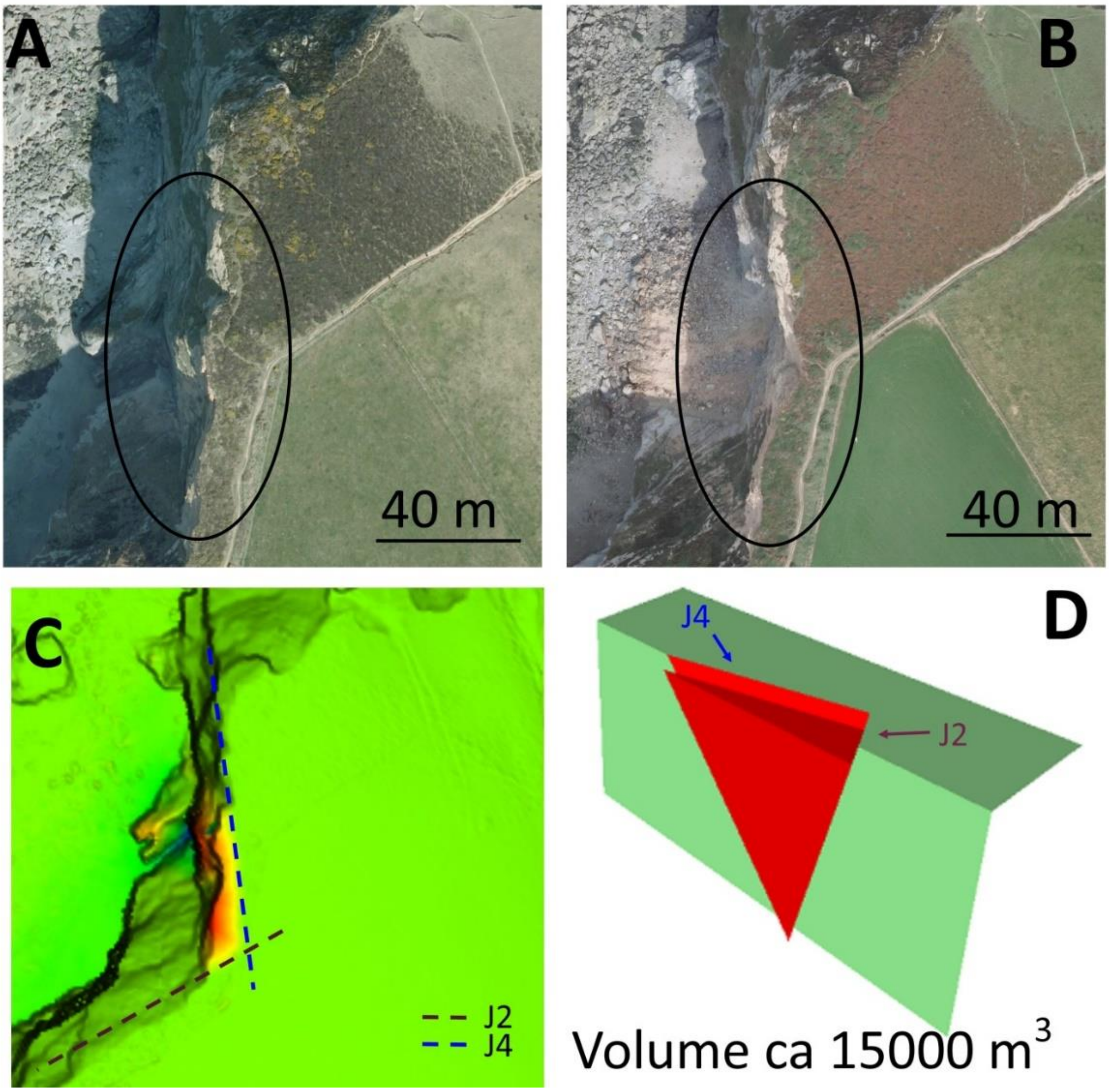

Figure 15. Basset's Cove failure. A) Basset's Cove slope before the failure. B) Basset's Cove slope after the failure. C) Comparison of 2011 and 2014 LiDAR data and structural features. D) Simplified conceptual 3D model of the Basset's Cove failure (View towards North-East).

4.5 Results from GIS kinematic analysis

GIS kinematic analysis confirmed that the interaction of F1, F2 and F4 play a key role in the evolution and in the control of failures along this section of the North coast. Figures 16 A and B show respectively the slope and the aspect maps used for the analysis and Figures 17 and 18 show potential locations along the coastline that are susceptible to possible planar failures along F1 and wedge failures along F1/F2 and F4. Also shown in these figures are photographs taken of previous landslides (dominated by F1, F2 and F4) observed in the study area between Hell’s Mouth and Portreath. Validation of the observed failures is discussed in more depth in the following section.

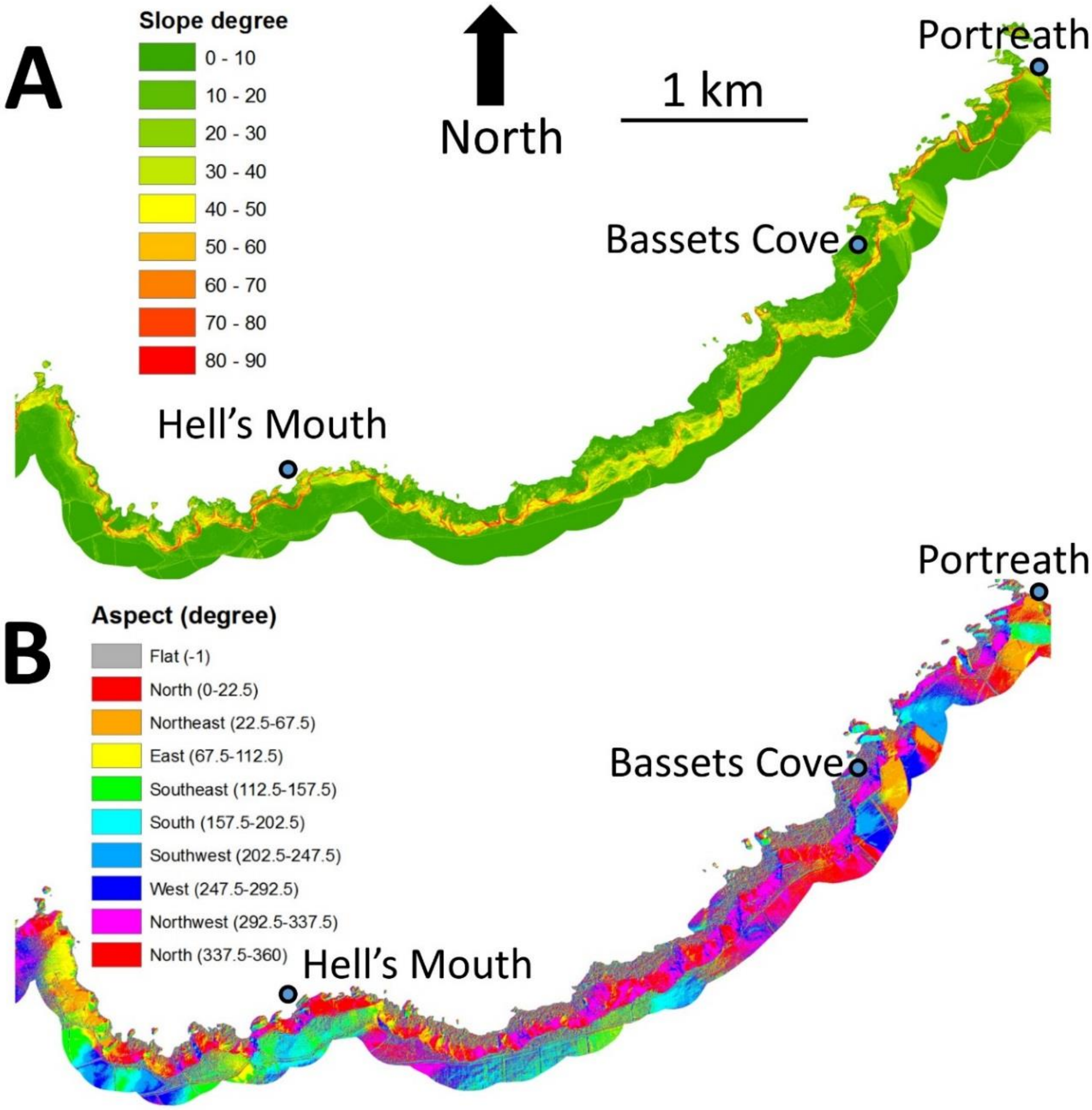

Figure 16. Thematic maps. A) Slope inclination or dip map. B) Slope aspect or dip direction map.

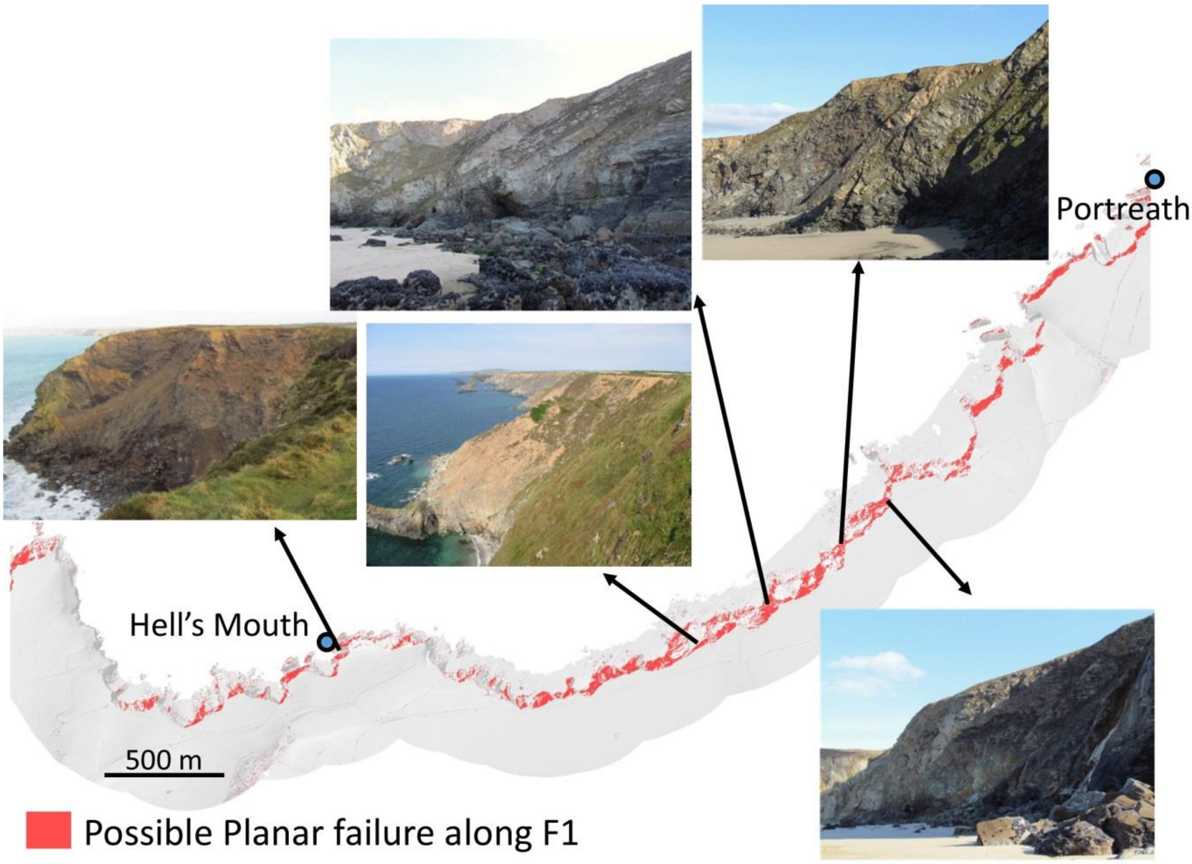

Figure 17. Results obtained by GIS kinematic instability test for slopes that may be prone to planar failure and example photographs of previous landslides in the area.

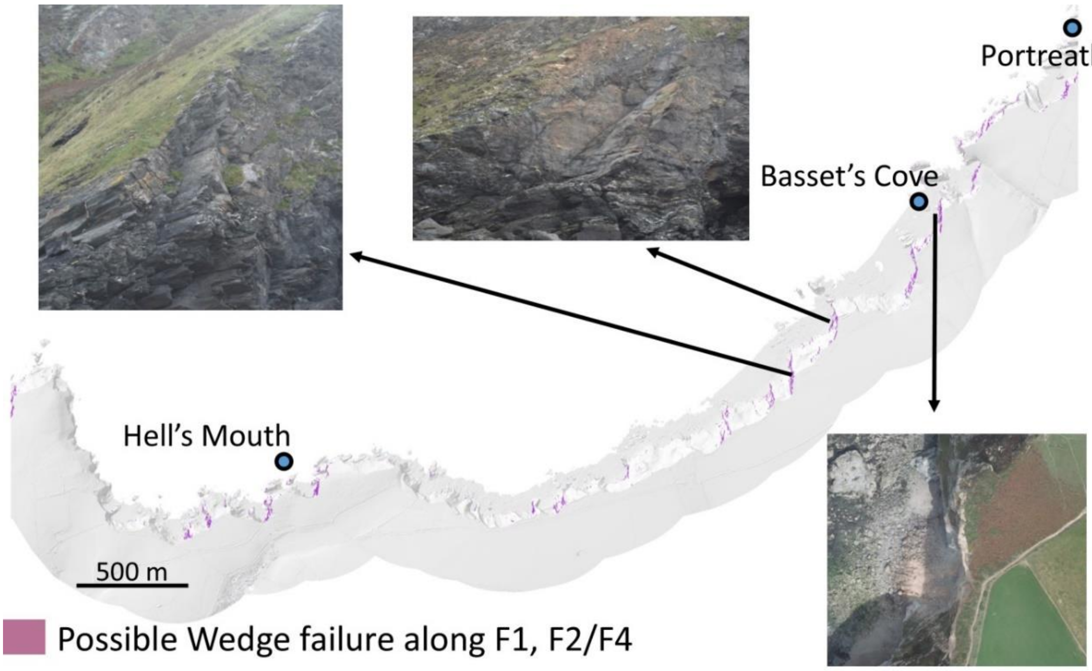

Figure 18. Results obtained by GIS kinematic instability test for slopes that may be prone to wedge failure and example wedge failure photographs from the study area.

5 Validation of the Results

In order to validate the results of the GIS kinematic instability evaluation on-site ground-truthing has been performed for a section of coastline that could be safely accessed at low tide. A three-dimensional model of the section of coastline was generated from 800 photographs using structure from motion (SfM) techniques. The point cloud model consisted of 30 million points, creating a dense reconstruction of the foreshore and cliff face. This dataset was then orientated and taken into SplitFX, where feature or discontinuity orientation mapping was performed for verification of discontinuity-controlled instability. Figure 19A illustrates the three-dimensional point cloud model in context with the case study area, Figure 19B example feature mapping undertaken in SplitFX and Figure 19C the resultant polar contour stereonet of mapped discontinuities. The discontinuity orientations mapped agree well with previous engineering geology mapping and remotely mapped features shown in Figures 4 and 5.

Photographs of previous discontinuity-controlled instabilities, and their location along the coastline, highlighted in Figures 17 and 18, were also identified in the point cloud and orientations of the major discontinuities obtained from SplitFX for validation purposes. Figure 20 shows the dip and dip direction of discontinuities associated with both planar and wedge failure showed in Figure 17 and 18 for the respective failures, highlighting the controlling influence of F1, F2 and F4. Figure 20 also demonstrates the scale of different failure modes and the controlling influence of structural geology. For example, planar failures shown in Figures 17 and 20 are associated with F1 and can affect the entire cliff section, generating large failures (i.e. Hell’s Mouth failure). Whereas, wedge failures are associated with F4 and F1/F2 (and related fracture sets) and tend to generate smaller volume failures (shown in Figures 18 and 20). Due to health and safety reasons, access to Basset’s Cove area (Figure 15 and bottom right image in Figure 18) was restricted and therefore the authors performed structural analysis utilizing the aerial LiDAR dataset for validation (Figure 15).

How it is possible to observe in Figure 20 and as previously discussed, type and scale of failure vary in relation to the structural control.

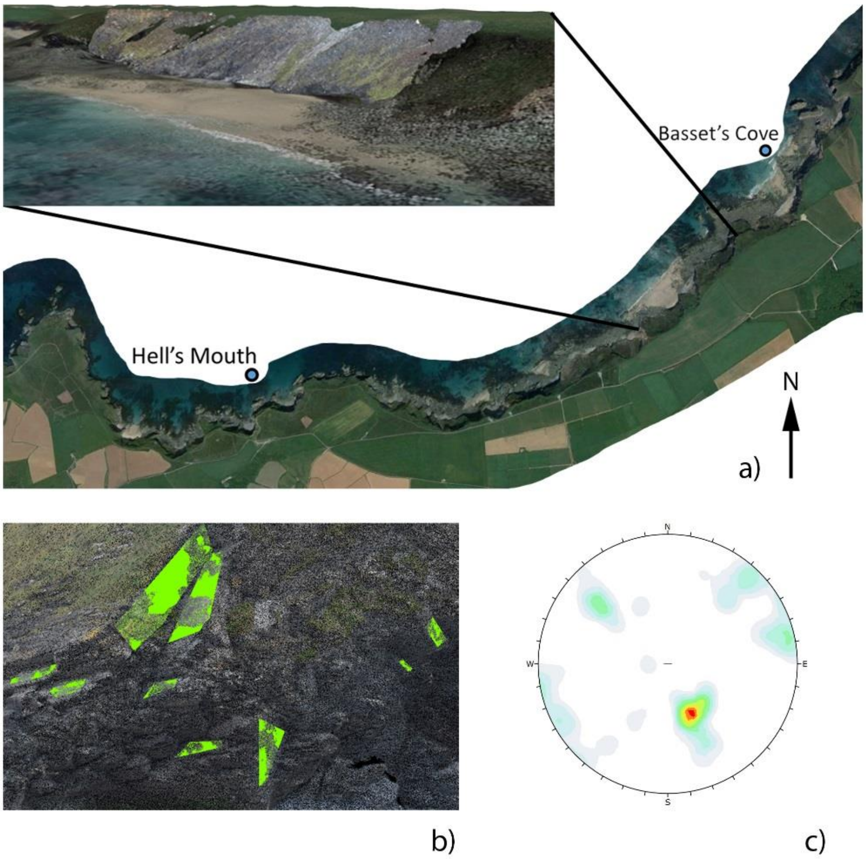

Figure 19. a) Area of validation mapping and location of the structure from motion (SfM) generated point cloud b) close up images of the SfM model and example discontinuity mapping c) lower hemisphere polar contour stereonet of discontinuities identified from SplitFX mapping.

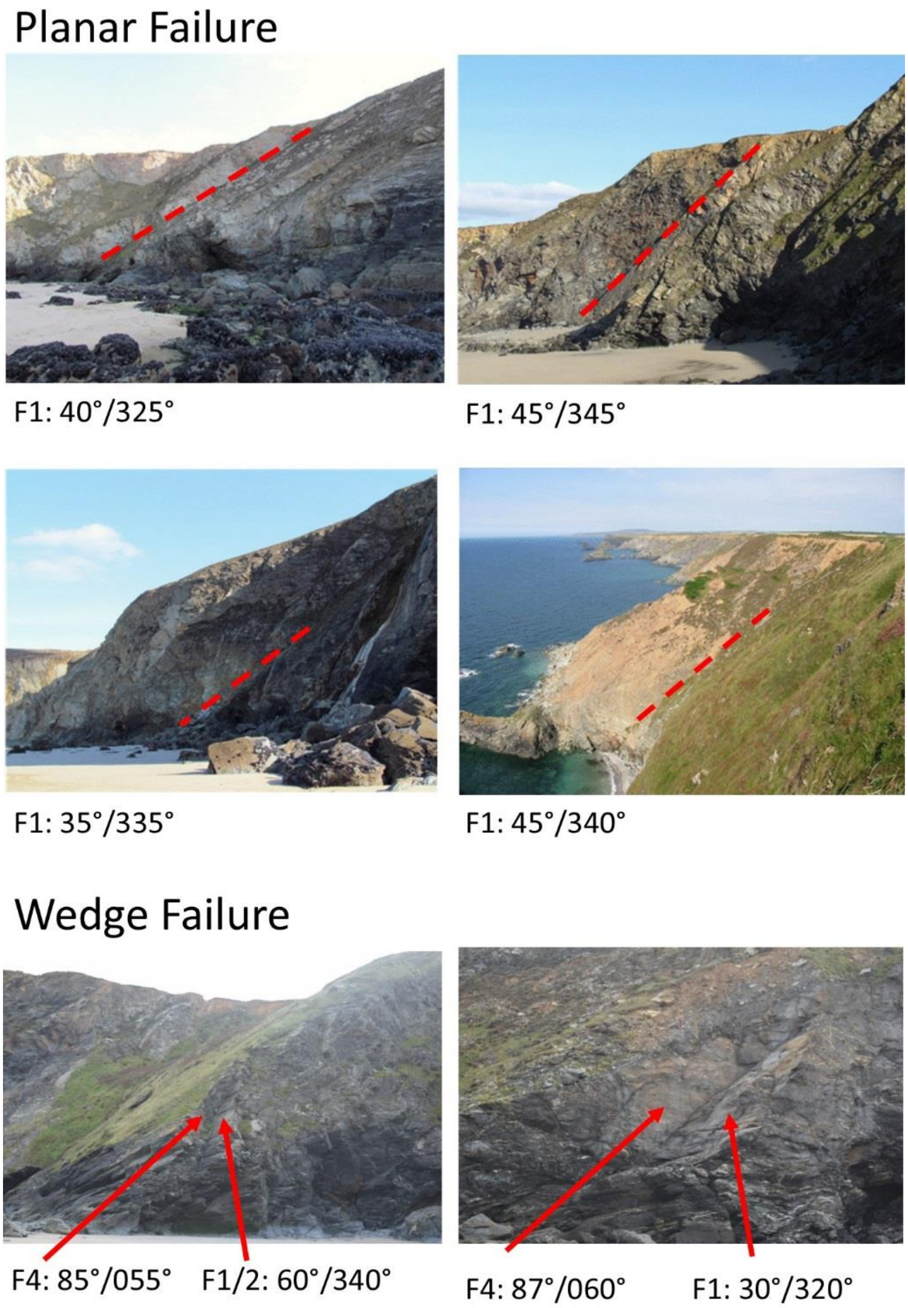

Figure 20. Orientation of discontinuities controlling both planar and wedge failure for selected photographs from Figures 17 and 18.

6 Discussion

Previous applications of aerial surveys alone have not provided the necessary detail needed in engineering-based analysis in coastal areas (Lim et al. 2005). This paper has highlighted the benefits that can be achieved from a combined engineering geological – structural geology approach for mapping and characterization of blocky rock mass coastlines. Aerial LiDAR surveys have been used to remotely obtain the major geological structures of the surrounding coastline in order to gain an understanding of the factors influencing the numerous failures that have occurred on the North Coast of Cornwall, UK. The spatial coverage of the aerial LiDAR survey allows the user to explore large sections of the coastline and provides the basis for an initial scoping study to highlight unstable areas that may require more detailed in-depth evaluation using terrestrial based survey techniques.

In view of the restricted access to the failure site at Hell's Mouth, limited safe access to the toe of the cliff and the steep nature of the coastal section a variety of remote mapping techniques were used to collect the structural data for discontinuity set characterization. This included use of both terrestrial laser scanning from accessible locations (although these were not ideal, being rather oblique to the failure) and use of long-range photogrammetry from an adjacent headland (use of both f = 200 and 400 mm focal length lenses). Although, the survey method and subsequent data processing techniques used are similar to those highlighted by Lim et al. (2005), Mitasova et al. (2009) and Obu et al. (2016) the photogrammetric and laser scanning was non-optimal due to unavoidable occlusion related to the rather oblique point of view. Occlusion in the datasets resulted in both the terrestrial LiDAR and photogrammetric models poorly representing oblique structures. Relying on this information alone, has the potential to bias the results. By incorporating a long range photogrammetric survey from the opposite headland, occlusion was improved but areas of the point cloud were still obscured by the surrounding geometry of the coastal outcrops. This suggests that a combination of approaches and set-up locations is best suited to the case study at Hell's Mouth.

This problem, rather typical in coastal and very steep slopes has been discussed by Rosser et al. (2005), Sturzenegger and Stead (2009) and Francioni et al. (2017b) and was overcome by Michoud et al. (2015) by use of boat-based mobile laser scanning along a coastal cliff section in Normandy. In the case of the North Coast location future research will include the use of UAV surveys similar to those highlighted by Francioni et al. (2015), Salvini et al. (2015) and Colomina and Molina (2014). During the investigation features measured/identified with terrestrial remote sensing techniques were classified as discontinuities since it is not possible to identify kinematic indicators in the DTP models. For this reason, features obtained from remote sensing surveys have been termed generally as discontinuities. It is however clear that some major features such as listric faults can be identified during these types of survey.

In the case of the Hell's Mouth study, the registration of the high resolution photogrammetric datasets generated a model consisting of approximately 30 million points. This high-resolution model allowed identification of discontinuity features in Split FX. Manual assignment of ‘patches’ and ‘traces’ was found to be preferable to the automated extraction of features that provides orientation of surfaces from point-normal clustering that may identify features that are not fractures or discontinuities. This is due to the complex mesh generation required in the study area rather than using the Triangulated Irregular Network (TIN) available in Split FX as discussed by Gigli and Casagli (2011). In addition, manual operation allowed the authors to verify the selection and allocation of discontinuity surfaces using ‘patches’, while also having the ability to identify daylighting features using ‘trace planes’. This minimisess interpretation errors and allows measurement of fracture spacing and persistence of identified features.

This research has used different remote sensing based platforms, both terrestrial and aerial, to identify areas of coastal instability. Multi-temporal aerial LiDAR has been used to provide an initial scoping study to identify areas of coastal instability and major structures that could influence failure. In addition, the incorporation of the aerial LiDAR data into a GIS-based workflow provides the basis for a desk-based kinematic instability analysis of the study area. The use of both long range and short range photogrammetric and laser scanning techniques provided useful complementary data for discontinuity identification. The long range photogrammetry was a useful low-cost alternative to terrestrial LiDAR; in this case a long-range laser scanner instrument located at the adjacent headland would have to be used at considerable capital expenditure. When comparative studies were undertaken the discontinuity set identification from both the terrestrial laser scanning imagery and photogrammetric reconstruction in this study provided similar eigenvalues (mean pole for identified set(s)) to previous comparative studies (Coggan et al. 2007). In addition, following deviation analysis undertaken in CloudCompare, similar accuracies (150 mm deviation in overlapping areas where occlusion from TLS was not present) were achieved to that from previous research by James and Robson (2012) and Westoby et al. (2012). However, accurate geo-referencing of both laser scanning and photogrammetric reconstructions can be problematic in coastal areas, where consistent periodic targets between surveys are hard to relocate due to erosion, human intervention and the inability to install new stations. In this case study, the authors established a DGNSS (Differential Global Navigation Satellite System) baseline away from the coastal path utilizing pre-existing infrastructure with a positional error of approximately 5 mm. The established baseline was then used for periodic survey control to mitigate against re-establishment errors.

The Hell’s Mouth landslide investigation clearly highlights that instability problems on the North Coast of Cornwall are directly related to the pre-existing geological structure along the blocky rock mass coastline. Rosser et al. (2007) also showed similar findings where concentration of failures occurred along small scale rock mass structure features (e.g. bedding planes, or low persistent joints) although their study was on a smaller scale (a few kilometres of coastline). Smaller rockfall events appeared to be related to less persistent discontinuities, resulting in kinematic instability.

The study of the North Coast of Cornwall is at a larger regional scale and has highlighted that larger failures, such as that observed near Hell's Mouth, for coastline sections striking NE-SW, are the result of high persistence low-angle first order listric faults (F1) interacting with higher angle first order faults and sub-parallel joint sets (F4/J4 and F2/J2). Initial time-lapse video analysis of the Hell's Mouth failure by Stead et al. (2012) highlighted the importance of joint dilation and fracturing immediately prior to the failure suggesting that the failure mechanisms may be complex and likely involved interaction of several 1st order faults and lower order discontinuity sets with degradation and damage of the rock mass preceding failure. The observed failure itself involved considerable rock mass fragmentation and intact rock fracture. It must be noted that the failure models presented in this research provide a simplistic representation of the Hell's Mouth failure. It can be seen in the video of the collapse, that the failure is more complex. The fracturing of rock bridges and the interaction of highly persistent slope dipping faults (F1) with other fault systems (F2 and F4) and with smaller less persistent joint sets could also contribute to failure. Further analysis with numerical methods and analysis of additional data from UAV surveys will be carried out in future to explore the complexity of the observed failure. These observations regarding potential complex mechanisms can be extended to other large planar failures shown in Figures 17 and 20, where failures occur along F1 with F2/J2 and F4/J4 act as tension cracks and lateral release surfaces respectively. The planar failures could be also defined as wedge failures, with F1 acting as the basal plane. With regards to wedge analysis (shown in Figures 18 and 20) both pure wedge failures, related to the interaction between F4 and F1, and more complex wedge failure generated by a series of smaller wedges/blocks or retrogressive failures associated with intersections between F2/J2 and F4/J4 (e.g. Basset's Cove failure, Figures 15 and 18) were observed.

7 Conclusion

The North Coast of Cornwall, UK, is susceptible to landslide processes, varying from low volume rock fall to entire cliff collapse. This investigation shows a combined engineering geological – structural geology approach incorporating structural analysis, remote sensing and GIS analysis. This approach is highly suited for preliminary analysis of landslide susceptibility in blocky rock coastlines, varying from large (e.g. Hell's Mouth) to relatively small scale (e.g. Basset's Cove) failures.

Engineering geological analysis of the area, carried out through conventional and remote sensing surveys, showed the presence of five discontinuity sets and four first order fault systems. The mapped discontinuities can be directly related to the geological evolution of the area, and mainly reflect two dominant trends: NW-SE and NE-SW respectively.

GIS analysis highlighted that the coastline orientation and the current tension crack orientations mapped immediately behind the crest of the Hell's Mouth landslide also align with these two main structural trends, suggesting that coastal evolution is strongly controlled by the structural geology of the area. On-site validation of GIS kinematic indicators was undertaken using photographs and discontinuity mapping from structure from motion (SfM) generated point cloud data.

A comparison of the 2011 and 2014 aerial LiDAR data highlighted two failures that occurred in the study area during the intervening time period; one in close proximity to Hell's Mouth and the other at Basset's Cove. The analysis of these failures showed that they are directly related to the structural geology of the area. However, the volume of the failures can vary considerably depending on the coastline orientation and the discontinuities involved. Listric faults dipping NW (associated with discontinuity set F1/J1) have dip magnitudes varying from low to high angles and can generate large volume landslides in cliffs with adverse orientations. In such cases, discontinuities related to sets F2/J2 and F4/J4 act as tension cracks and lateral release surfaces respectively. Smaller volume landslides can also occur along the intersection of sub-vertical faults related to F4 and F1/F2.

LiDAR comparison of point cloud data, integrated with GIS analyses and field engineering geology survey data, has allowed an improved understanding of potential failure mechanisms that control coastal instability. The combined use of LiDAR and photogrammetry played an important role in this research as most of the coastline area under study is very difficult to access due to the steep nature of the rugged cliffs with limited foreshore accessibility. Integration of conventional field engineering geological surveys with remote sensing techniques allowed the authors to analyze a larger section of the coastal area and produce a data set representative of the entire portion of the coast (including inaccessible areas). This work has provided a basis for improved understanding the role of discontinuities and major faults (structural geology) on coastal instability that have occurred\occurring in the area.

Acknowledgements

The authors wish to thank Mr. Louis Robert Guy Penfound-Marks (University of Exeter, Camborne School of Mines) for his support during the engineering geological survey. Moreover, we would like to express our gratitude to the reviewers who provided important and constructive suggestions for improving the quality of the paper.

References

Abellán, A., Jaboyedoff, M., Oppikofer, T., Vilaplana, J.M. 2009. Detection of millimetric deformation using a terrestrial laser scanner: Experiment and application to a rockfall event. Natural Hazards and Earth Surface Science. 9, 365-372.

Agisoft. 2016. Agisoft Photoscan: http://www.agisoft.com/

Alexander, A.C., Shail, R.K. 1995. Late Variscan structures on the coast between Perranporth and St. Ives, Cornwall. Proceedings of the Ussher Society, 8, 398-404.

Brideau M-A, Yan, M., Stead, D. 2009. The role of tectonic damage and brittle rock fracture in the development of large rock slope failures. Geomorphology. 103, (1), 30-49.

Brideau M.A., Pedrazzini A., Stead D., Froese C., Jaboyedoff M., van Zeyl D. 2011. Three-dimensional slope stability analysis of South Peak, Crowsnest Pass, Alberta, Canada. Landslides, 8, 139-158.

British Geological Survey. 2017. http://www.bgs.ac.uk/landslides/

Channel Coastal Observatory. 2017. http://www.channelcoast.org/

Collins, B.D., Sitar, N., 2011. Stability of steep slopes in cemented sands: Journal of Geotechnical and Geoenvironmental Engineering. 137, 43-51.

Coggan, J.S., Wetherelt, A., Gwynn, X.P., Flynn, Z. 2007. Comparison of hand-mapping with remote data capture systems for effective rock mass characterisation, 11th Congress of International Society for Rock Mechanics, Lisbon 2007, 9th - 13th Jul 2007, Proceedings of 11th Congress of the International Society for Rock Mechanics - the second half century of rock mechanics, 1, 201-205.

Colomina, I. and Molina, P., 2014.Unmanned aerial systems for photogrammetry and remote sensing: A review. ISPRS Journal of Photogrammetry and Remote Sensing, 92, pp.79-97.

CloudCompare v2.6, GPL software. 2016. Retrieved from http://www.cloudcompare.org/.

Dickson, M.E., Perry, G.L.W. 2016. Identifying the controls on coastal cliff landslides using machine-learning approaches. Environmental Modelling & Software. 76, 117-127.

ESRI 2016. ArcMap version 10.2: http://www.esri.com/arcgis/about-arcgis.

Fey, C., Rutzinger, M., Wichmann, V., Prager, C., Bremer, M., Zangerl, C. 2015. Deriving 3D displacement vectors from multi-temporal airborne laser scanning data for landslide activity analyses. GIScience & Remote Sensing. 52 (4), 437-461.

Francioni, M., Salvini, R., Stead, D., Giovannini, R., Riccucci, S., Vanneschi, C. and Gullì, D. 2015. An integrated remote sensing-GIS approach for the analysis of an open pit in the Carrara marble district, Italy: Slope stability assessment through kinematic and numerical methods. Computers and Geotechnics 67: 46-63.

Francioni, M., Stead, D., Clague, J.J., Westin, A. 2017(a). Identification and analysis of large paleo-landslides at Mount Burnaby, British Columbia. Environ Eng Geosci. https://doi.org/10.2113/EEG-1955.

Francioni, M., Salvini, R., Stead, D., Coggan, J. 2017(b). Improvements in the integration of remote sensing and rock slope modelling. Nat Hazards. In Press. https://doi.org/10.1007/s11069-017-3116-8.

Gigli, G., Casagli, N. 2011. Semi-automatic extraction of rock mass structural data from high resolution LIDAR point clouds, In International Journal of Rock Mechanics and Mining Sciences. 48 (2), 187-198.

Hoek, E. and Bray, J.W., 1981. Rock slope engineering, third edition. The Institution of Mining and Metallurgy, London, 358 pp.

Hollick, L.M., Shail R.K., Leveridge B.E. 2006. Devonian rift-related sedimentation and Variscan tectonics – new data on the Looe and Gramscatho basins from the resurvey of the Newquay district. Geoscience in south-west England, 11, 191-198.

Hughes, S.P., Stickland, R.J., Shail, R.K., LeBoutillier, N.G., Alexander, A.C. and Thomas, M. 2009. The chronology and kinematics of late Palaeozoic deformation in the NW contact metamorphic aureole of the Land's End Granite. Geoscience in South-West England, 12, 140-152.

Humair, F., Pedrazzini, A., Epard, J.-L., Froese, C.R., Jaboyedoff, M. 2013. Structural characterization of Turtle Mountain anticline (Alberta, Canada) and impact on rock slope failure. Tectonophysics 605, 133-148.

James, M.R. and Robson, S. 2012. Straightforward reconstruction of 3D surfaces and topography with a camera: Accuracy and geoscience application. Journal of Geophysical Research, Vol. 117.

Jaboyedoff M, Baillifard F, Couture R, Locat J, Locat P. 2004. Toward preliminary hazard assessment using DEM topographic analysis and simple mechanic modeling. In: Lacerda

WA, Ehrlich M, Fontoura AB, Sayo A (eds) Proceedings of the 9th International symposium on landslides. Balkema, Rotterdam, pp 191-197

Jones, D.K.C., Griffith, J.S. and Lee, E.M. 1988. The distribution of recorded landslides in south-west England. Proceedings of the Ussher Society, 7, 91-92.

Rocscience. 2016. Dips V7, SWedge V6. https://www.rocscience.com/

Leveridge, B.E. 2011. The Looe, south Devon and Tavy Basins: the Devonian rifted passive margin successions. Proceedings of the Geologists' Association, 122, 616-717.

Leveridge, B.E. and Hartley, A.J. 2006. The Variscan Orogeny: The development and deformation of Devonian/Carboniferous basins in SW England and South Wales. In: Brenchley, P.J. and Rawson, P.F. (eds) The Geology of England and Wales. The Geological Society, London, 226-237.

Leveridge, B.E. and Shail, R.K. 2011. The Gramscatho Basin, south Cornwall, UK: Devonian active margin successions. Proceedings of the Geologists' Association, 122, 568–615.

Lim, M., Petley, D. N., Rosser, N. J., Allison, R. J., and Long, A. J. 2005. Combined digital photogrammetry and time-of-flight laser scanning for monitoring cliff evolution. The Photogrammetric Record, 20(June), 109–129.

Mantovani, M., Devoto, S., Piacentini, D., Prampolini, M., Soldati, M.,Pasuto, A. 2016. Advanced SAR interferometric analysis to support geomorphological interpretation of slow-moving coastal landslides (Malta, Mediterranean Sea). Remote Sensing. 8(6), 443.

Markland, J.T. 1972. A useful technique for estimating the stability of rock slopes when the rigid wedge sliding type of failure is expected. Imperial College Rock Mechanics Research Reprints, 19 (10 pp.).

Mateos, R.M., Azañón, J.M., Roldán, F.J., Notti, D., Pérez-Peña, V., Galve, J.P., Pérez-García, J.L., Colomo, C.M., Gómez-López, G.M., Montserrat, O., Devantèry, N., Lamas-Fernández, F., Fernández-Chacón, F. 2017. The combined use of PSInSAR and UAV photogrammetry techniques for the analysis of the kinematics of a coastal landslide affecting an urban area (SE Spain). Landslides. 14 (2) 743-754.

Michoud, C., Carrea, D., Costa, S., Derron, M.H., Jaboyedoff, M., Delacourt, C., Maquaire, O., Letortu, P., Davidson, R. 2015. Landslide detection and monitoring capability of boat-based mobile laser scanning along Dieppe coastal cliffs, Normandy. 12 (2) 403-418.Mitasova, H., Overton, M.F., Recalde, J.J., Bernstein, D.J. and Freeman, C.W. 2009. Raster-based analysis of coastal terrain dynamics from multi-temporal lidar data. Journal of Coastal Research. 25(2), 507-514.

Naylor, L.A., Stephenson, W.J., Trenhaile, A.S., 2010. Rock coast geomorphology: Recent advances and future research directions. Geomorphology. 114, 3-11.

Obu, J., Lantuit, H., Grosse, G., Günther, F., Sachs, T., Helm, V. and Fritz, M. 2016. Coastal erosion and mass wasting along the Canadian Beaufort Sea based on annual airborne LiDAR elevation data. Geomorphology. In press. ttp://dx.doi.org/10.1016/j.geomorph.2016.02.014.

Oppikofer, T. 2009. Detection, analysis and monitoring of slope movements by high-resolution digital elevation models. PhD thesis, Institute of Geomatics and Analysis of Risk, University of Lausanne, Lausanne, Switzerland, 377 p.

Rosser, N. J., Lim, M., Petley, D.N. 2005. The use of terrestrial laserscanning for monitoring the process of hard rock coastal cliff erosion,Q. J. Eng. Geol. Hydrogeol., 35, 71-78.

Rosser, N., Lim, M., Petley, D., Dunning, S., and Allison, R. 2007. Patterns of precursory rockfall prior to slope failure. Journal of Geophysical Research: Earth Surface, 112, 10.

Rosser, N.J., Brain, M.J. Petley, D.N., Petley, Lim, M., Norman, E.C. 2013. Coastline retreat via progressive failure of rocky coastal cliffs. Geology 41 (8), 939-942.

Salvini, R., Riccucci, S., Gullì, D., Giovannini, R., Vanneschi, C., and Francioni, M. 2015. Geological application of UAV photogrammetry and terrestrial laser scanning in Marble quarrying (Apuan Alps, Italy). In Engineering Geology for Society and Territory (Vol. 5, pp. 979–983). Engineering Geology for Society and Territory. http://doi.org/10.1007/978-3-319-09048-1.

Shail, R.K., Coggan, J.S. and Stead, D. 1998. Coastal landsliding in Cornwall, UK: Mechanisms, modelling and implications. Proceedings of the eighth International Congress of the International Association for Engineering Geology and the Environment, held 21-25 September 1998, Vancouver, Canada, pp. 1323 - 1330.

Split Engineering LLC. 2016. Split-FX: https://www.spliteng.com/.

Stead, D., Jaboyedoff, M. and Coggan, J. 2012. Rock slope characterization and geomechanical modelling. Landslides and Engineered Slopes: Protecting Society through Improved Understanding, London, ISBN 978-0-415-62123-6.

Stock, G.M., Martel, S.J., Collins, B., Harp, E.L., 2012. Progressive failure of sheeted rock slopes: The 2009–2010 Rhombus Wall rock falls in Yosemite Valley, California, USA. Earth Surface Processes and Landforms. 37, 546-561.

Sturzenegger, M., Stead, D. 2009. Quantifying discontinuity orientation and persistence on high mountain rock slopes and large landslides using terrestrial remote sensing techniques. Natural Hazards and Earth System Sciences 9 (2), 267-287.

Xie, M., Esaki, T. and Cai M.F. 2004. A GIS-based method for locating the critical 3D slip surface in a slope. Computers and Geotechnics 31: 267-277.

Xie, M., Esaki, T., Qiu, C. and Wang C.X. 2006. Geographical information system-based computational implementation and application of spatial three-dimensional slope stability analysis. Computers and Geotechnics 33: 260-274.

Westgate, B.M. 2005. Development of a methodology for instability risk assessment for coastal slopes in Cornwall. PhD thesis, Camborne School of Mines (University of Exeter).

Westgate, B.M., Coggan, J.S. and Pine, R.J. 2003. Development of a risk-based approach to coastal slope instability assessment in Cornwall. Geoscience in south-west England, 10, 390-396.

Wolters, G., Müller, G., 2008. Effect of cliff shape on the internal stresses and rock slope stability. Journal of Coastal Research. 24, 43-50.

Westoby, M.J, Bradington, J. Glasser, N.F. Hambrey, M.J. and Reynolds J.M. 2012. ‘Structure-from-Motion’ photogrammetry: A low-cost, effective tool for geoscience applications. Geomorphology. 179, 300-314.

Van Westen, C.J., 1998. GIS in landslide hazard zonation: A view, with cases from the Andes of Colombia, in: Mountain Environment and Geographic Information Systems, F.P. Martin, D.I. Heywood (eds.). Taylor & Francis, London, pp. 35–165.